Surface & Coatings Technology 344 (2018) 102–110

Contents lists available at ScienceDirect

Surface & Coatings Technology

journal homepage: www.elsevier.com/locate/surfcoat

Vacuum heat treatment mechanisms promoting the adhesion strength of thermally sprayed metallic coatings

Guo-Hui Meng, Bang-Yan Zhang, Hong Liu*, Guan-Jun Yang*, Tong Xu, Cheng-Xin Li, Chang-Jiu Li

State Key Laboratory for Mechanical Behavior of Materials, School of Materials Science and Engineering, Xi'an Jiaotong University, Xi'an, Shaanxi 710049, PR China

ARTICLE INFO

Keywords:
Thermal spray
Vacuum heat treatment
Adhesion strength
Oxide film
Diffusion
Thermodynamic model

ABSTRACT

In this study, the mechanisms responsible for enhancing the adhesion strength of thermally sprayed metallic coatings subjected to vacuum heat treatment were investigated using atmospheric plasma sprayed (APS) CoNiCrAlY coatings as an example. The formation of metallurgical bonding between the coating and the substrate, which determined the increase in the adhesion strength of the coatings, was studied by analyzing the effect of morphological changes of the oxide film in the coating. The results showed that during the vacuum heat treatment process, the oxide film formed during the coating deposition gradually broke down and subsequently shrank into round-shaped oxide inclusions. After vacuum heat treatment, the adhesion strength of the coating improved significantly. The increase in the adhesion strength was caused by the formation of metallurgical bonding between the coating and the substrate. However, the prerequisite for the formation of metallurgical bonding was that the oxide film had to break during the vacuum heat treatment process. A thermodynamic 2D model based on the thermal grooving theory was proposed to explore the essential conditions for the breaking and shrinking of the oxide film. The results predicted by the 2D model and the experimental results were in good agreement with each other and indicated that at a given temperature, the breaking of the oxide film is directly related to its thickness.

1. Introduction

In order to ensure that the mechanical components used in harsh environments have enough service life, metallic protective coatings are usually deposited on their surfaces [1–4]. Metallic protective coatings can assist in maintaining the mechanical properties of the components while improving the resistance of the structural parts to external environmental damage [1]. In general, the successful application of metallic protective coatings for engineering usage depends strongly on the quality of adhesion between the coating and the substrate [5]. Low quality adhesion could lead to premature failure of the coating, which results in the structural parts being exposed to harsh environments, which in turn can cause serious damage [6].

Thermal spraying is a well-established technology and has been widely employed to deposit different types of metallic protective coatings [7]. In most cases, the adhesion between the thermal sprayed coating and substrate is attributed to the mechanical interlocking [8,9]. In addition, the interaction (adhesive interaction (Van der Waals forces) and/or metallurgical interaction (metallurgical bonding)) between the first splat and the substrate also contributes to the adhesion [5,8,10]. However, it must be noted that in the case of thermally sprayed metallic coatings, the first splat does not fully cover the substrate. The contact areas between the bottom of the first splat and the substrate are sometimes called welding points or active zones, which account for just about 20% to 30% of the entire splat area [8,11]. Moreover, in the contact zone, although metallurgical bonding is a strong form of bonding, its proportion in the contact area is very small [5,10]. In general, pores occupied most of the area between the splats and the substrate [12]. As pores can become the sources for cracks and act as channels for crack propagation, the adhesion strength of thermally sprayed metallic coatings is usually low.

Because adhesion strength determines the ability of the coating to resist spalling during service, much importance is attached to improving the adhesion strength of metallic coatings deposited by thermal spraying [3,6,13]. It is worth mentioning that vacuum heat treatment is widely used to improve the quality of metallic coatings [8,9]. One of the functions of vacuum heat treatment is to enhance the adhesion strength of the coating. Richard et al. [6] reported that during vacuum heat treatment, the metallic coating contacted the metallic substrate, leading to a diffusion of elements between the two components. This

* Corresponding authors.
E-mail addresses: hongliu@mail.xjtu.edu.cn (H. Liu), ygj@mail.xjtu.edu.cn (G.-J. Yang).

https://doi.org/10.1016/j.surfcoat.2018.03.010
Received 26 October 2017; Received in revised form 3 March 2018; Accepted 6 March 2018
Available online 06 March 2018
0257-8972/

results in a decrease in the porosity and an increase in the proportion of metallurgical bonding in the active zone. Therefore, the adhesion strength of a coating can be improved by vacuum heat treatment. However, it is worthwhile to note that during the coating deposition process in ambient conditions, the sprayed particles inevitably come into contact with oxygen during flight in the flame jet and eventually a layer of metal oxide is formed around the molten particles [14]. Even in the case of metallic coatings deposited by vacuum plasma spray, it has been shown that the molten particles reacted with the residual oxygen in the vacuum device and formed an oxide layer, a few tens of nanometers thick, on the surface of the splat [2]. Evans et al. [15] confirmed that the presence of an oxide film prevents the diffusion of metallic elements and results in the single splat coated by the oxide film becoming an isolated diffusion core unit. In other words, if an oxide film exists on the splat surface, it is difficult to enhance metallurgical bonding between the coating and the substrate via vacuum heat treatment. However, a large number of studies have reported that the adhesion strength of the metallic coatings deposited by thermal spraying improved significantly after vacuum heat treatment [6,8,9]. There are differences between the theoretical and experimental results. Further research is therefore required to understand the root causes for such differences.

After vacuum heat treatment, the adhesion strength of the metallic coatings changes significantly. The answer to this question may be that the oxide film, which acts as a barrier to the diffusion of metallic elements, undergoes changes during the vacuum heat treatment process. Therefore, it is necessary to investigate this issue by focusing on the changes in the diffusion barrier. However, in the case of a coating deposited in a low oxygen atmosphere (such as vacuum plasma spray), the oxide film may be too thin to observe the changes in the diffusion barrier. On the other hand, as a metallic protective coating with good resistance to high temperature corrosion and oxidation, CoNiCrAlY coatings deposited by different thermal spray processes have been widely studied and many reports focused on improving the adhesion strength of these coatings by vacuum heat treatment [8,9,16,17]. Therefore, in this study, considering atmospheric plasma-sprayed CoNiCrAlY coatings as an example, the changes in the diffusion barrier of oxide film during the vacuum heat treatment process were studied. It is found that the morphology of the oxide film changed significantly during the heat treatment process. With an increase in the heat treatment time, the oxide film gradually broke down and shrank into round-shaped oxide inclusions. After the oxide film broke down, metallurgical bonding between the coating and the substrate was enhanced, which led to an increase in the adhesion strength of the coating.

2. Experimental procedures

2.1. Preparation of coatings

First of all, disc-shaped specimens, 25.4 mm in diameter and 3 mm in thickness, were cut from a cylindrical rod made up of a nickel-based superalloy Inconel-738 using spark erosion. The nominal composition (in wt%) of this superalloy (NCS) was listed in Table 1. Because this study focused mainly on the reason behind the metallurgical bonding between the coating and the substrate during vacuum heat treatment and the effect of metallurgical bonding alone on the adhesion strength of the coating, it was necessary to eliminate any interference by other factors. Although roughened substrates are used in practice, heat treatment might alter the mechanical interlocking between the coating and the substrate, thus affecting the improvement in the adhesion strength of the coating due to metallurgical bonding. Therefore, it was necessary to use mirror-polished substrates. This approach was followed in a large number of investigative efforts on the morphology of single splats and the bonding between the splats and polished substrates [10,18–20]. At the same time, it is easier to observe the changes in the bonding between the coating and substrate using polished substrates. In summary, we chose a polished alloy as the substrate. Therefore, prior to coating deposition, the substrate was prepared by successive grinding and polishing. Grinding was carried out using 1200 grit SiC abrasive paper. Polishing was performed using a paste of 1.5 μm and 0.25 μm diamond grains. After grinding and polishing, these specimens were thoroughly cleaned ultrasonically with isopropanol and dried by blowing with compressed nitrogen gas.

A commercial spraying powder of CoNiCrAlY (Amdry 9951, Oerlikon Metco, Switzerland) was selected for coating deposition. This powder was produced by argon atomization and contained spherical particles with a mean particle size of 25.8 μm (d_{10} = 12.9 μm and d_{90} = 38.6 μm). The nominal composition (in wt%) of this powder (NCP) was listed in Table 2. Later, a 350 μm-thick CoNiCrAlY coating was deposited on the as prepared superalloy surface using a commercial atmospheric plasma spraying system (GP-80, Jiu Jiang, China). The torch used for coating deposition was a machine-mount torch (9MBM, Oerlikon Metco, Switzerland). During coating deposition, 12 passes were completed to achieve the thickness of 350 μm. The specific spray conditions were listed in Table 3.

2.2. Vacuum heat treatment

Vacuum heat treatment experiments were performed in an industrial vacuum furnace (SBF 966H, EXEMOO, China) at 1373 K (a temperature commonly used in the vacuum heat treatment of the thermal sprayed MCrAlY bond coat [21,22]). The specimens were placed in an annealed alumina crucible and transported to the hot zone of the furnace. The coating/superalloy system was then heated to 1373 K at a heating rate of 4 K/min when the furnace pressure was below 1×10^{-3} Pa. The exposure time of different specimens was varied between 4 h and 10 h at 1373 K. After the heat treatment, the specimens were allowed to cool in vacuum to the ambient temperature at a cooling rate of 4 K/min.

2.3. Characterization

The type of bonding (mechanical bonding or metallurgical bonding) between the coating and substrate has a great influence on the adhesion strength of the coating and usually the adhesion strength of a coating can be qualitatively characterized by the type of bonding [3,8]. Therefore, it is necessary to characterize the type of bonding of the coating-substrate interface before and after vacuum heat treatment. Electron backscattered diffraction (EBSD) is a commonly used method to characterize the grain boundary and grain orientation of materials, based on which the type of bonding between the coating and substrate can be judged. In the case of thermally sprayed metallic coatings, in the active zones, metallurgical bonding between the as-sprayed coating and the substrate is mainly due to the melting of the substrate [3,8]. After

Table 1
EDS test results (in wt%) of the substrate.

Elements	Ni	Cr	Co	Al	Ti	W	Mo	Ta	Nb	C	Zr	B
NCS	61.57	16	8.5	3.5	3.25	2.6	1.75	1.75	0.8	0.17	0.1	0.01
S1	62.16	15.9	8.3	3.4	3.31	2.5	1.73	1.71	0.7	0.18	0.1	0.01
S2	62.06	15.9	8.4	3.4	3.18	2.5	1.66	1.83	0.8	0.16	0.1	0.01

Table 2
EDS test results (in wt%) of the powder/splat.

Elements	O	Al	Co	Ni	Cr	Y
NCP	–	7.95	38.79	31.72	21.03	0.51
P1	24.75	31.89	15.09	14.67	10.91	2.69
P2	28.47	37.58	13.29	11.24	7.47	1.95
P3	23.51	30.77	16.56	15.86	11.89	1.41
P4	–	7.91	38.74	31.01	21.71	0.63

Table 3
Plasma spraying parameters.

Parameters	Value
Arc current (A)	600
Arc voltage (V)	65
Primary plasma gas (Ar/slpm)	30
Secondary plasma gas (H_2/slpm)	1
Powder feed gas (N_2/slpm)	5
Powder feed rate(g/min)	30
Spray distance (mm)	80
Traverse speed of torch (mm/s)	800

the coating is deposited on the surface of the polished substrate, in the melting region, strong metallurgical bonding is formed and there is no continuous straight interface between the coating and the substrate. Moreover, if the sprayed material has a crystal structure similar to that of the substrate, epitaxial growth can be found between some grains of the coating and the substrate [3]. In this study, we used the EBSD (Aztec, Oxford Instruments, United Kingdom) technique to characterize the type of bonding of the CoNiCrAlY coating-substrate interface. In addition, in order to characterize the microstructure and composition of the coating/superalloy system, a field emission scanning electron microscope (MIRA 3 LMH, TESCAN, Czech Republic), equipped with an energy dispersive X-ray spectrometer (Aztec, Oxford Instruments, United Kingdom) was employed to generate secondary electron (SE) images, backscattered electron (BSE) images, and EDS test data. Before the cross-sections of the specimen can be characterized, appropriate metallographic specimens should be prepared. The cross-sections of the specimens were prepared as follows. Initially, the entire coating/superalloy system was vacuum-impregnated for 1 h in a two-component epoxy (EpoThin 2, Buehler, USA). Later, after curing the epoxy for 24 h in air at room temperature, the coating/superalloy system was sectioned perpendicular to the coating surface using an automatic precise cutting machine (IsoMet HS, Buehler, USA). Finally, the cross-sections were ground and polished as described previously.

2.4. Adhesion strength testing

The specimens for measuring the adhesion strength of the coating were divided into three groups – without vacuum heat treatment, 4 h of vacuum heat treatment at 1373 K, and 10 h of vacuum heat treatment at 1373 K. The adhesion strength of the coating was evaluated in accordance with the ASTM C633-01 standard. Five identical cylinder couples and five specimens were selected from each group for testing. The specimen was bonded in the middle of the two cylinders using resin glue (Adbest, HUA YI Resins Co., China). Subsequently, the glued cylinders were mounted in a tensile test machine (Instron 1195, Instron, USA) equipped with a self-aligning fixture. Each specimen was subjected to a tensile load at a constant rate of 1 mm/min until the coating peeled off.

3. Results

3.1. Surface and cross-sectional characteristics of the as-sprayed CoNiCrAlY coatings

Fig. 1(a) exhibits the surface characteristics of the as-sprayed CoNiCrAlY splat deposited on the polished superalloy substrate. The initial spherical molten particle transformed into a round splat after hitting the substrate. Although the Inconel-738 superalloy has the same crystal structure as the CoNiCrAlY powder, the BSE image showed that the contrast of the surface of the splat was dissimilar to that of the substrate. It can be seen in Fig. 1(a) that the surface of the splat was darker than that of the substrate. The results of EDS point analysis (point S1 in Table 1 and point P1 in Table 2) showed that the Al and O contents on the surface of the splat were high, which indicated that the surface of the splat was coated with a layer of alumina.

Fig. 1(b) shows the surface characteristics of the as-sprayed CoNiCrAlY coating. The deposited particles spread on the surfaces of the previously deposited splats due to which the coating exhibited a layer by layer packing feature. It is worth noting that the contrast between splats and the contrast even within the same splat were different. The results of EDS point analysis (point P2 and point P3 in Table 2) showed that the types of elements present in different contrast regions of this splat were basically the same and the Al and O contents were higher than those of other elements. However, the Al and O contents in the darker areas (point P2) were about 21% higher than those in the brighter areas (point P3). This might mean that the surface of the splat was coated with a thin layer of alumina but the thickness of the alumina film varied.

Fig. 2 shows the cross-sectional microstructure of the as-sprayed CoNiCrAlY coating. As shown in Fig. 2(a), a large number of alumina films existed in the coating. These alumina films were relatively continuous and smooth but their thickness was not uniform. The oxide film indicated by the arrow in Fig. 2(a) exhibited that the thickness of the alumina film was usually greater at both ends of the film. A small region in the interface between the first splat and the substrate (Fig. 2(b)) showed close contact between the coating and the substrate; there was no apparent formation of an alumina film in this region unlike in other

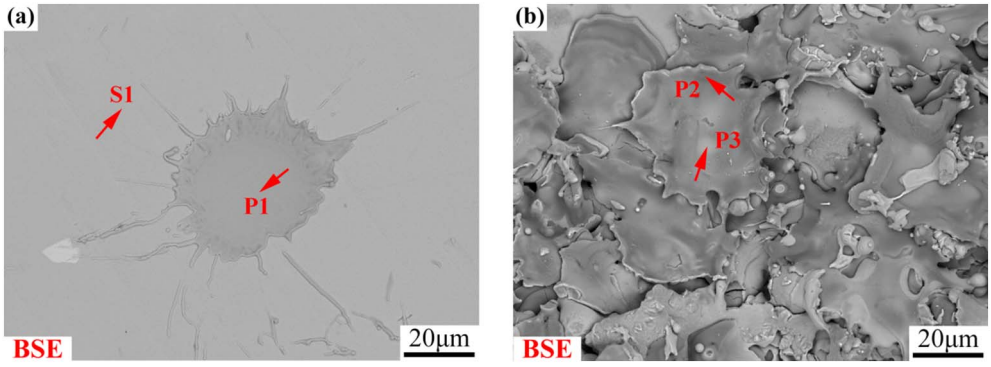

Fig. 1. Surface characteristics of the (a) as-sprayed CoNiCrAlY splat and (b) coating.

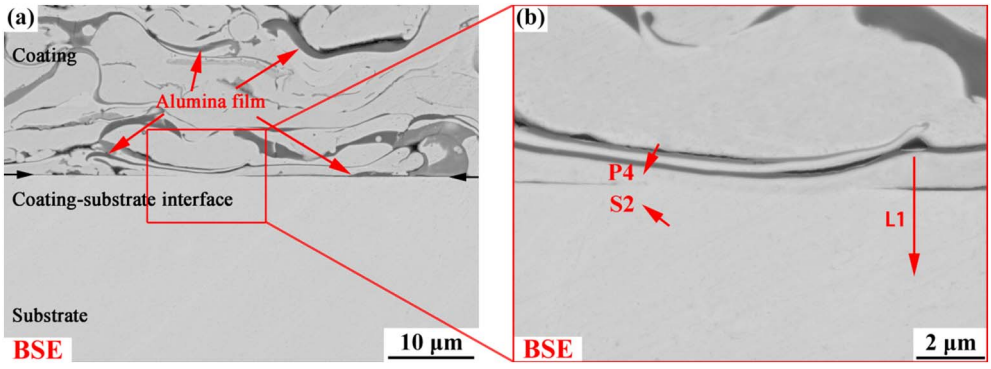

Fig. 2. Cross-sectional microstructure of the as-sprayed CoNiCrAlY coating.

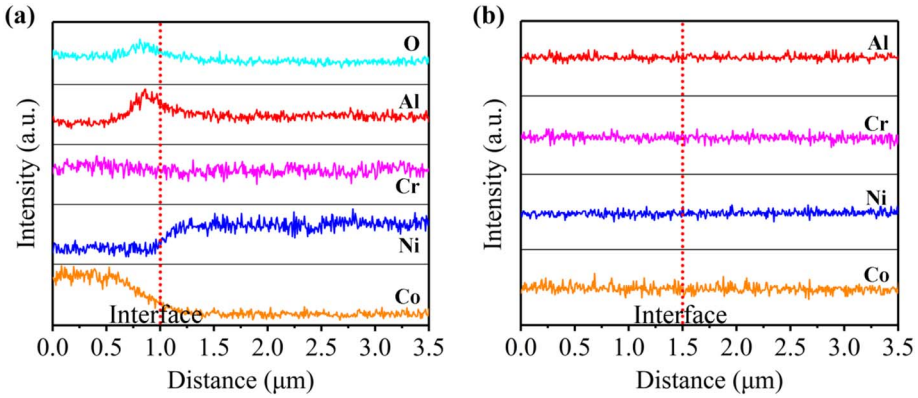

Fig. 3. Distribution of elements near the coating-substrate interface: (a) as-sprayed coating in Fig. 2(b) and (b) 4 h heat-treated coating in Fig. 6(a).

regions. As shown in Fig. 3(a), EDS line analysis results indicated that the contents of Cr, Ni, and Co elements on both sides of the alumina film were different. On the coating side, the Cr and Co contents were higher while the Ni content was greater on the substrate side. This difference was consistent with the chemical composition of the splat (point P4 in Table 2) and the substrate (point S2 in Table 1). This might mean that there was no obvious diffusion of elements between the as-sprayed coating and the substrate.

Fig. 4 exhibits the EBSD results of the interface between the as-sprayed CoNiCrAlY coating and the polished Inconel-738 superalloy substrate. It can be seen in Fig. 4(b) and (c) that the grain size of the splats was small with an average grain size of 0.97 μm. Moreover, there were a number of unresolved regions in the oxide film. It is worthwhile to note that there was a clear and continuous straight interface between the coating and the substrate, even at the position in Fig. 4(a) where a better combination could be observed. This might mean that the substrate was not melted by the molten particles. In addition, although the Inconel-738 superalloy has the same crystal structure as the CoNiCrAlY coating, no obvious epitaxial growth was found between the grains of the coating and the substrate. The above results might mean that a strong metallurgical bonding was not formed between the as-sprayed coating and the substrate.

3.2. Cross-sectional characteristics of the CoNiCrAlY coating after vacuum heat treatment

Fig. 5(a) shows the cross-sectional microstructure of the CoNiCrAlY coating after 4 h of vacuum heat treatment. The initial smooth thick alumina film in the coating became uneven, showing a clear jagged shape. However, the thin alumina film transformed into oval-shaped alumina inclusions with discontinuous distribution. At the interface between the coating and the substrate, there were a number of small round spots. These spots were found to be alumina by EDS analysis (Fig. 6(b)). Moreover, it could be observed that the Al, Co, Ni, and Cr contents in the coating and the substrate between these round-shaped alumina inclusions were consistent (Fig. 3(b)). These experimental

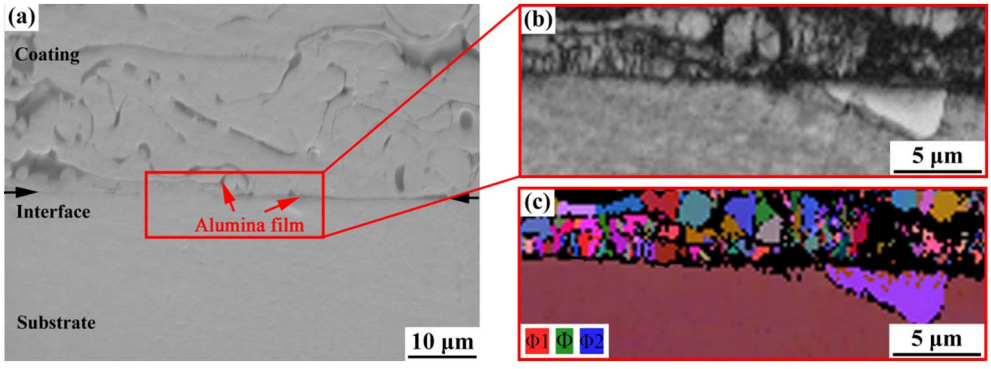

Fig. 4. EBSD results of the as-sprayed CoNiCrAlY coating: (a) original image, (b) grain morphology, and (c) orientation image.

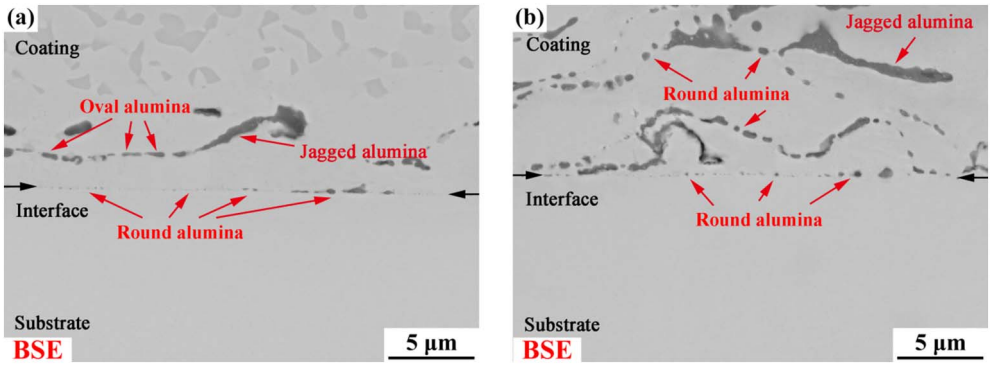

Fig. 5. Cross-sectional images of the microstructure of heat-treated CoNiCrAlY coatings: (a) 4 h treatment and (b) 10 h treatment.

results demonstrated that the morphology of the alumina film changed significantly and that a diffusion of elements occurred between the coating and the substrate during vacuum heat treatment.

Fig. 5(b) shows the cross-sectional microstructure of the CoNiCrAlY coating after 10 h of vacuum heat treatment. Compared to the coating treated for 4 h (Fig. 5(a)), the alumina film obtained after heat treating the coating for 10 h exhibited greater changes in its morphology. In the coating, oval-shaped alumina inclusions were few in number, while the number of round-shaped alumina inclusions was large. In addition, at the interface between the coating and the substrate, these alumina inclusions were almost all round in shape. This might mean that the morphology of the alumina film will change further with an increase in the treatment time. However, it is worth noting that at some positions where the alumina film was thick, it exhibited a jagged shape. The reasons for such changes would be described in detail in the next section.

Fig. 7 shows the EBSD results of the interface between the coating and substrate after 4 h of vacuum heat treatment. As shown in Fig. 7(b) and Fig. 7(c), the average grain size of the splat was 2.32 μm, which was larger than that of the coating without vacuum heat treatment (Fig. 4). At the position between these alumina grains, some grains of the splat exhibited the same orientation as the substrate grain. This made the grains of the substrate look as though they were penetrating the coating and the interface between the coating and the substrate become uneven. Compared to the coating without vacuum heat treatment (Fig. 4), the type of bonding of the coating-substrate interface changed significantly after vacuum heat treatment. A strong metallurgical bonding might have been formed between the coating and the substrate during vacuum heat treatment.

3.3. Adhesion strength of the CoNiCrAlY coating before and after vacuum heat treatment

In order to quantitatively characterize the effect of vacuum heat treatment on the adhesion strength of thermally sprayed metallic coatings, the adhesion strength of the CoNiCrAlY coating before and after vacuum heat treatment was analyzed and the results were shown in Fig. 8. Obviously, the adhesion strength of the CoNiCrAlY coating increased greatly after heat treatment. The adhesion strength of the coating without heat treatment was 28 MPa. After 4 h of heat treatment, it increased to 57 MPa. When the heat treatment time was further extended to 10 h, the adhesion strength increased to 66 MPa. It is worth noting that the adhesion strength of the coating subjected to 4 h of heat treatment was almost twice as large as that of the coating without heat treatment. However, the difference between the adhesion strengths of the 10 h and 4 h treated coatings was only 16%. The reasons for such differences would be described in detail in the next section.

In order to understand the mechanism behind the increase in the adhesion strength of thermally sprayed metallic coatings subjected to vacuum heat treatment, after the coating was peeled off from the substrate surface during the adhesion strength test, we further studied the features of the surface of the substrate. As shown in Fig. 9, there were splats remaining on the surface of the substrate. The area ratio of the residual coating to the entire substrate was shown in Fig. 8. It was obvious that after vacuum heat treatment, the proportion of the residual coating increased. In the coating without heat treatment, the area ratio of the residual coating was 51%. After 4 h of heat treatment, this ratio increased to 75%. When the heat treatment time was extended to 10 h, the ratio increased to 78%. As can be clearly seen in Fig. 8, the trends corresponding to the increase in the adhesion strength and the area ratio of residual coating with heat treatment time were similar. This meant that the number of splats remaining on the surface of the substrate may indirectly indicate the magnitude of the adhesion strength.

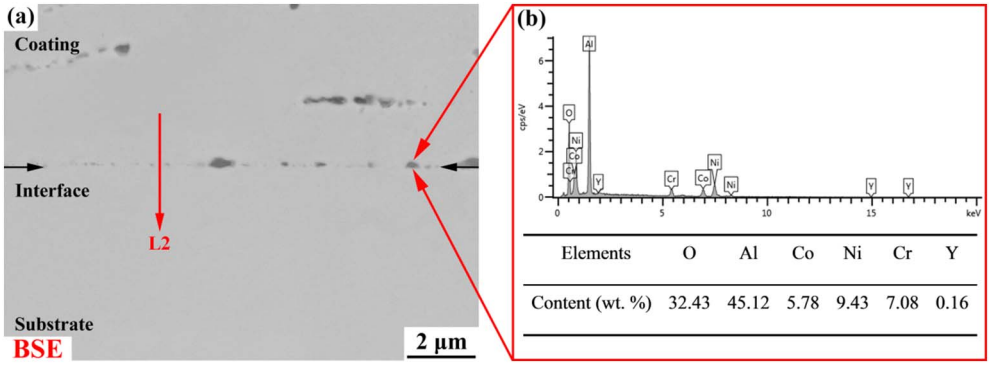

Fig. 6. EDS results of the CoNiCrAlY coating after 4 h of vacuum heat treatment.

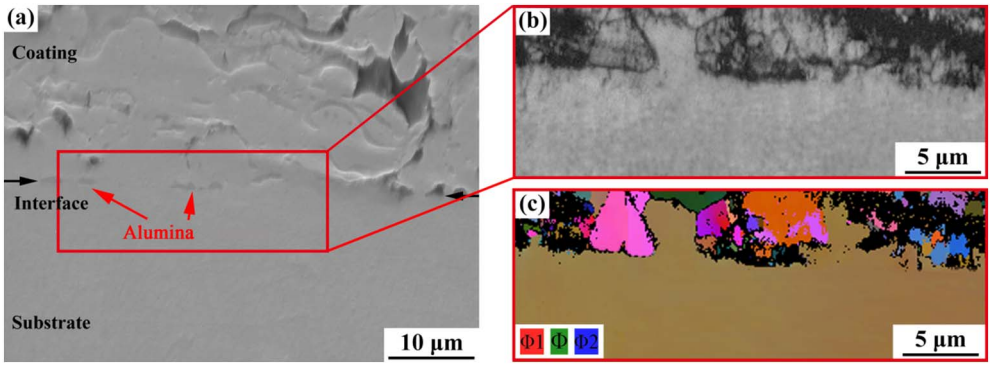

Fig. 7. EBSD results of the CoNiCrAlY coating after 4 h of vacuum heat treatment: (a) original image, (b) grain morphology, and (c) orientation image.

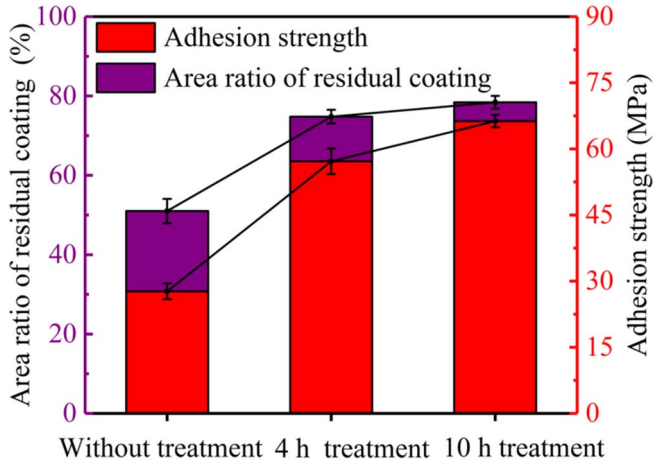

Fig. 8. Area ratio of residual coating and adhesion strength of CoNiCrAlY coatings.

4. Discussion

4.1. Morphology evolution mechanisms of the oxide film during vacuum heat treatment

One of the most significant changes in the coating after vacuum heat treatment was the morphological changes of the oxide film. With an increase in the treatment time, the oxide film changed from a smooth film (Fig. 2) to discontinuous oval-shaped oxide inclusions and eventually into round-shaped oxide inclusions (Fig. 5). Such morphological changes in the oxide film indicated that the oxide film underwent breaking and shrinking during vacuum heat treatment. It is well known that during high temperature treatment, thermal grooves will emerge from the surface of the metal or ceramic [23–27]. The surface of the metal or ceramic became uneven after the formation of thermal grooves, which was consistent with the experimental results observed in Fig. 5. Therefore, in this study, a thermodynamic 2D model based on the thermal groove theory was developed to explore the essential conditions for the breaking and shrinking of the oxide film. Based on this thermodynamic model, the morphological changes of the oxide film and their effect on the adhesion strength of the coating were discussed.

Fig. 10 depicts the thermodynamic 2D model and its evolution during the vacuum heat treatment. As shown in Fig. 10(a), the 2D model assumed that there was an oxide film of uniform thickness (H) at the coating-substrate interface (corresponding to the oxide film in Fig. 2). In this oxide film, two contact oxide grains were rectangular and had the same width (D). Moreover, the grain boundary energy (γ_{gb}) between the two oxide grains, the interfacial energy (γ_{i_c}) between the oxide grains and the coating, and the interfacial energy (γ_{i_s}) between the oxide grains and the substrate were isotropic. Under this condition, the interfacial and grain boundary energies were in a state of non-equilibrium at the junction positions. As shown in Fig. 10(b), at high temperature, in order to achieve equilibrium, the diffusion of atoms through the oxide grains took place; consequently, the grain boundary and interfacial energies tended to balance out and at the same time, the energy of the whole system was lowered. For a given area, a round grain has the smallest perimeter compared to any other grain; therefore, the oxide grain shrank into a round grain (in actual 3D cases, the grain shrank into a sphere). Taking the junction position between the oxide grains and the coating as an example, this position was in a state of thermodynamic equilibrium when the interfacial energy (γ_{i_c}) and the grain boundary energy (γ_{gb}) satisfied Eq. (1).

$$2\gamma_{i_c}\sin\theta_c = \gamma_{gb} \tag{1}$$

θ_c is the contact angle between the oxide grains and the coating at the junction position. At this point, according to the principle of constant quality, the depth of the thermal groove (δ_c) could be calculated using Eq. (2).

$$\delta_c = \frac{D(\theta_c - \cos\theta_c \sin\theta_c)}{4\sin^2\theta_c} \tag{2}$$

Similarly, the depth of the thermal groove (δ_s) at the junction position between the oxide grains and the substrate could be calculated using Eq. (3).

$$\delta_s = \frac{D(\theta_s - \cos\theta_s \sin\theta_s)}{4\sin^2\theta_s} \tag{3}$$

As shown in Eq. (4), when the sum of these two groove depths (δ) was higher than the original thickness (H) of the oxide film, the oxide film broke down. Otherwise, the morphology of the oxide film will remain intact.

$$\delta = \delta_c + \delta_s = \frac{D(\theta_c - \cos\theta_c \sin\theta_c)}{4\sin^2\theta_c} + \frac{D(\theta_s - \cos\theta_s \sin\theta_s)}{4\sin^2\theta_s} > H \tag{4}$$

As shown in Fig. 10(c), after the breaking down of the oxide film, the oval-shaped oxide inclusions continued to shrink into round-shaped oxide inclusions in order to further minimize the energy of the system (corresponding to the round-shaped oxide inclusions in Fig. 5).

The experimentally observed changes in the morphology of the oxide film during vacuum heat treatment can be explained using this 2D model. It can be inferred from the above equations that the breaking of the oxide film exhibited a linear relationship with the thickness of the oxide film. In addition, because the breaking and shrinking of the oxide film is a thermodynamically driven diffusion process, there is a positive relationship between the quantity of diffused elements and the diffusion time [25,28]. Therefore, for oxide films of different thickness values, under the same processing temperature and time, the breaking process was completed earlier for the thinner oxide film. At this moment, the thicker oxide film still maintained continuity, but its morphology became uneven. In this study, as shown in Fig. 5(a), for the coating

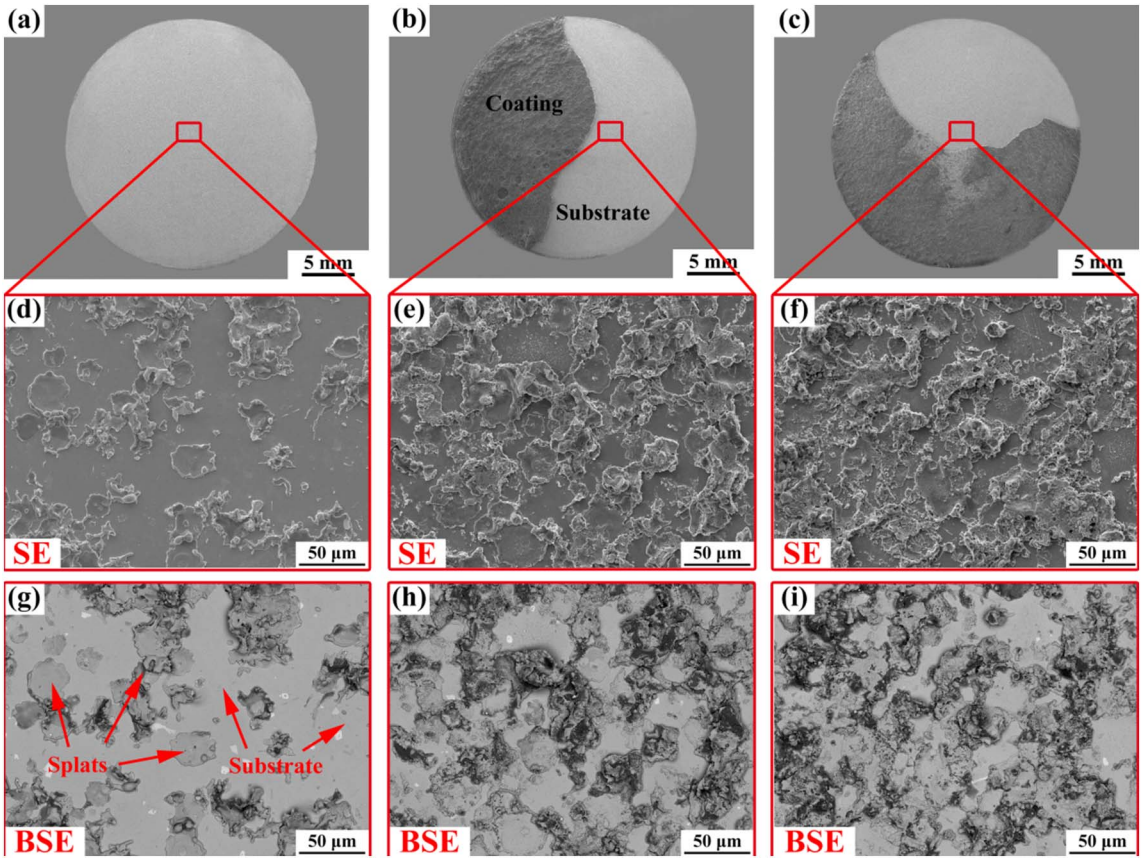

Fig. 9. Surface features of the substrate before and after vacuum heat treatment: (a), (d), and (g) without treatment, (b), (e), and (h) 4 h treatment, (c), (f), and (i) 10 h treatment.

subjected to 4 h of heat treatment, the thinner oxide film at the coating-substrate interface broke earlier and shrank into round-shaped oxide inclusions. In the case of the thicker oxide film in the coating, the oxide film also broke but compared to the thinner oxide film at the coating-substrate interface, it did not undergo a long shrinking period and thus resulted in oval shapes. When the heat treatment time was increased to 10 h as shown in Fig. 5(b), the round-shaped oxide inclusions at the coating-substrate interface remained round in shape. However, in the coating, the oval-shaped oxide inclusions further shrank and finally transformed into round-shaped oxide inclusions. Therefore, in the coating subjected to 10 h of heat treatment, most of the oxide inclusions were round in shape. It is worth noting that beyond a certain thickness of the oxide film, even if the coating treatment time was increased to 10 h, oxide films with jagged shapes could still be detected. This is because the thickness of the oxide film exceeded the critical depth of the thermal grooves. As shown in Eq. (4), when the interfacial energy and the grain boundary of the junction position reached a state of equilibrium, the depth of the thermal grooves did not change. If the

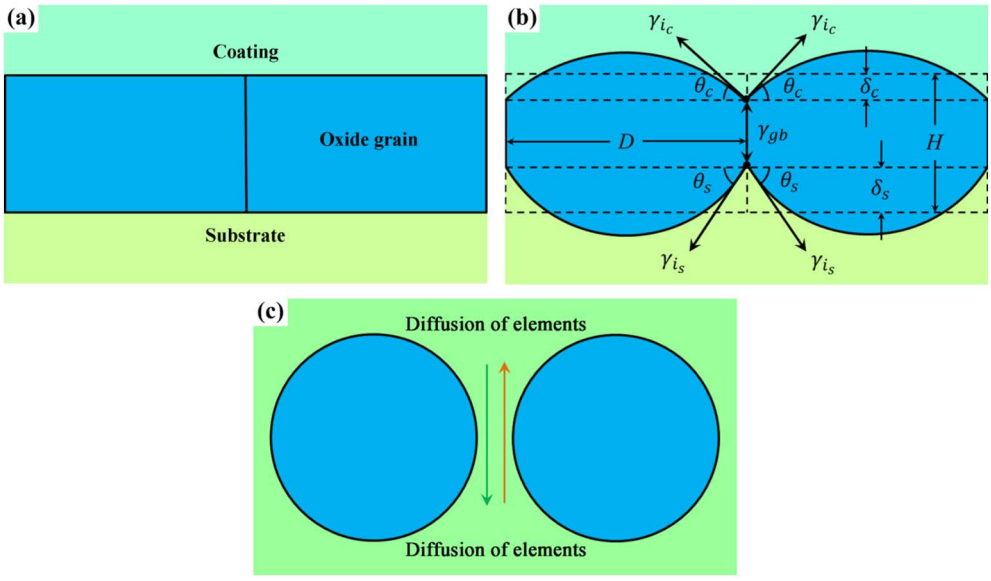

Fig. 10. Schematic illustration of the breaking and shrinking of the oxide film.

sum of these two groove depths is lower than the height of the oxide film, the oxide film would not break and the morphology of the oxide film would remain unchanged even if the processing time is prolonged. The theoretical results obtained using the thermodynamic 2D model on the breaking and shrinking of the oxide film were in good agreement with the experimental results.

4.2. Specific mechanisms of vacuum heat treatment promoting the adhesion strength of thermally sprayed metallic coatings

During the breaking and shrinking of the oxide film, the metal atoms of the coating and the substrate diffused along the surface of the oxide grains and occupied the space of the thermal grooves. When the thermal grooves on both sides of the oxide film came into contact with each other, a contact between the coating metal and the substrate metal was generated. As shown in Fig. 10(c), at high temperatures, diffusion of elements occurred between the coating and the substrate. The experimental results shown in Fig. 3(b) and Fig. 6 confirmed this view. Furthermore, as shown in Fig. 7, the grain size of the heat-treated splats was larger than the grain size of the untreated splats (Fig. 4). At the position between these alumina grains, some grains of the splat had the same orientation as the substrate grains. These experimental results might also indicate that after the oxide film broke down, inter-diffusion of elements between the coating and the substrate occurred. This is because inter-diffusion of elements between the coating and the substrate made the grains of the splats merge with each other and continue to grow during the heat treatment process. Therefore, after vacuum heat treatment, the grain size of the splats was larger than that of the untreated splats. Similarly, the grains between the coating and the substrate also merged with each other; this resulted in the grains of the substrate looking as though they penetrated the splats and the interface between the coating and the substrate becoming uneven. In summary, after vacuum heat treatment, the inter-diffusion of elements between the coating and substrate took place and the prerequisite for such inter-diffusion was that the oxide film had to break during the vacuum heat treatment process.

After the breaking of the oxide film, the inter-diffusion of elements resulted in the formation of metallurgical bonding between the coating and the substrate. The formation of metallurgical bonding firmly attached the splats to the surface of the substrate and they were not easy to peel off. Therefore, after vacuum heat treatment, the amount of residual splats increased significantly (Fig. 9) and the adhesion strength of the coating improved (Fig. 8). It is worth noting that the adhesion strength of the coating subjected to 4 h of heat treatment was almost twice as large as that of the coating without heat treatment. However, the difference between the adhesion strengths of the 10 h and 4 h treated coatings was only 16%. The reason for this phenomenon might be explained as follows. In the case of the coating subjected to 4 h of heat treatment, in most contact areas, the breaking of the thinner oxide film at the coating-substrate interface was already completed and the metallurgical bonding was formed between the coating and the substrate. Therefore, even if the heat treatment time was extended to 10 h, the type of bonding between the coating and the substrate did not change greatly (Fig. 5). In other words, the breaking and shrinking of the oxide film during vacuum heat treatment determined the relationship between the treatment time and the adhesion strength of thermally sprayed metallic coatings. As the breaking of the oxide film was directly related to its thickness, in practice, for thermally sprayed metallic coatings, the parameters (temperature and/or time) of the vacuum heat treatment process should be set according to the thickness of the oxide film.

5. Conclusions

1. In the case of metallic coatings deposited by thermal spraying in ambient atmosphere, an oxide film of variable thickness existed between the coating and the substrate.
2. With an increase in the heat treatment time, the oxide film formed during the coating deposition gradually broke down and subsequently shrank into round-shaped oxide inclusions.
3. The prerequisite for the formation of metallurgical bonding between the coating and the substrate was that the oxide film had to break during the vacuum heat treatment process.
4. At a given temperature, the breaking of the oxide film was directly related to its thickness.

Acknowledgments

This work was supported by the National Science Foundation of China (Grant No. 51671159); the Fundamental Research Funds for the Central Universities and the National Program for Support of Top-notch Young Professionals.

References

[1] G. Goward, Protective coatings - purpose, role, and design, Mater. Sci. Technol. 2 (1986) 194–200.
[2] B.Y. Zhang, G.H. Meng, G.J. Yang, C.X. Li, C.J. Li, Dependence of scale thickness on the breaking behavior of the initial oxide on plasma spray bond coat surface during vacuum pre-treatment, Appl. Surf. Sci. 397 (2017) 125–132.
[3] J.J. Tian, S.W. Yao, X.T. Luo, C.X. Li, C.J. Li, An effective approach for creating metallurgical self-bonding in plasma-spraying of NiCr-Mo coating by designing shell-core-structured powders, Acta Mater. 110 (2016) 19–30.
[4] E. Hejrani, D. Sebold, W.J. Nowak, G. Mauer, D. Naumenko, R. Vassen, W.J. Quadakkers, Isothermal and cyclic oxidation behavior of free standing MCrAlY coatings manufactured by high-velocity atmospheric plasma spraying, Surf. Coat. Technol. 313 (2017) 191–201.
[5] V.V. Sobolev, J.M. Guilemany, J. Nutting, J.R. Miquel, Development of substrate-coating adhesion in thermal spraying, Int. Mater. Rev. 42 (1997) 117–136.
[6] C.S. Richard, G. Béranger, J. Lu, J.F. Flavenot, The influences of heat treatments and interdiffusion on the adhesion of plasma-sprayed NiCrAlY coatings, Surf. Coat. Technol. 82 (1996) 99–109.
[7] A. Vardelle, C. Moreau, J. Akedo, H. Ashrafizadeh, C.C. Berndt, J.O. Berghaus, M. Boulos, J. Brogan, A.C. Bourtsalas, A. Dolatabadi, M. Dorfman, T.J. Eden, P. Fauchais, G. Fisher, F. Gaertner, M. Gindrat, R. Henne, M. Hyland, E. Irissou, E.H. Jordan, K.A. Khor, A. Killinger, Y.C. Lau, C.J. Li, L. Li, J. Longtin, N. Markocsan, P.J. Masset, J. Matejicek, G. Mauer, A. McDonald, J. Mostaghimi, S. Sampath, G. Schiller, K. Shinoda, M.F. Smith, A.A. Syed, N.J. Themelis, F.L. Toma, J.P. Trelles, R. Vassen, P. Vuoristo, The 2016 thermal spray roadmap, J. Therm. Spray Technol. 25 (2016) 1376–1440.
[8] L. Pawlowski, The Science and Engineering of Thermal Spray Coatings, John Wiley & Sons, 2008.
[9] P.L. Fauchais, J.V.R. Heberlein, M.I. Boulos, Thermal Spray Fundamentals, Springer US, 2014.
[10] S. Brossard, P.R. Munroe, A. Tran, M.M. Hyland, Study of the splat-substrate interface for a NiCr coating plasma sprayed onto polished aluminum and stainless steel substrates, J. Therm. Spray Technol. 19 (2010) 24–30.
[11] H.D. Steffens, B. Wielage, J. Drozak, Interface phenomena and bonding mechanism of thermally-sprayed metal and ceramic composites, Surf. Coat. Technol. 45 (1991) 299–308.
[12] C.J. Li, G.J. Yang, C.X. Li, Development of particle interface bonding in thermal spray coatings: a review, J. Therm. Spray Technol. 22 (2013) 192–206.
[13] V. Pershin, M. Lufitha, S. Chandra, J. Mostaghimi, Effect of substrate temperature on adhesion strength of plasma-sprayed nickel coatings, J. Therm. Spray Technol. 12 (2003) 370–376.
[14] S. Deshpande, S. Sampath, H. Zhang, Mechanisms of oxidation and its role in microstructural evolution of metallic thermal spray coatings—case study for Ni-Al, Surf. Coat. Technol. 200 (2006) 5395–5406.
[15] H.E. Evans, M.P. Taylor, Diffusion cells and chemical failure of MCrAlY bond coats in thermal-barrier coating systems, Oxid. Met. 55 (2001) 17–34.
[16] K. Ogawa, K. Ito, T. Shoji, D. Seo, H. Tezuka, H. Kato, Effects of Ce and Si additions to CoNiCrAlY bond coat materials on oxidation behavior and crack propagation of thermal barrier coatings, J. Therm. Spray Technol. 15 (2006) 640–651.
[17] K.V. Dahl, J. Hald, A. Horsewell, Interdiffusion between Ni-based superalloy and MCrAlY coating, Defect. Diffus. Forum 258–260 (2006) 73–78.
[18] Y.Z. Xing, Z. Liu, G. Wang, X.H. Li, Y.L. Xing, C.P. Jiang, Y.N. Chen, X.D. Song, M. Dargusch, Effects of spray parameters on the adhesion between plasma-sprayed cast iron splat and aluminium substrate, Surf. Coat. Technol. 315 (2017) 1–8.
[19] J. Wang, C.J. Li, G.J. Yang, C.X. Li, Effect of oxidation on the bonding formation of plasma-sprayed stainless steel splats onto stainless steel substrate, J. Therm. Spray Technol. 26 (2017) 47–59.
[20] A.A. Syed, A. Denoirjean, B. Hannoyer, P. Fauchais, P. Denoirjean, A.A. Khan, J.C. Labbe, Influence of substrate surface conditions on the plasma sprayed ceramic and metallic particles flattening, Surf. Coat. Technol. 200 (2005) 2317–2331.
[21] A. Weisenburger, G. Rizzi, A. Scrivani, G. Mueller, J.R. Nicholls, Pulsed electron beam treatment of MCrAlY bondcoats for EB-PVD TBC systems part 1 of 2: coating

production, Surf. Coat. Technol. 202 (2007) 704–708.
[22] J. Müller, D. Neuschütz, Efficiency of α-alumina as diffusion barrier between bond coat and bulk material of gas turbine blades, Vacuum 71 (2003) 247–251.
[23] T. Liu, X.T. Luo, X. Chen, G.J. Yang, C.X. Li, C.J. Li, Morphology and size evolution of interlamellar two-dimensional pores in plasma-sprayed $La_2Zr_2O_7$ coatings during thermal exposure at 1300 °C, J. Therm. Spray Technol. 24 (2015) 739–748.
[24] P.V. Mcallister, I.B. Cutler, Thermal grooving of MgO and Al_2O_3, J. Am. Ceram. Soc. 55 (1972) 351–354.
[25] W.W. Mullins, Theory of thermal grooving, J. Appl. Phys. 28 (1957) 333–339.
[26] S.K. Sharma, J. Spitz, Thermal grooving in thin silver films, J. Mater. Sci. 16 (1981) 535–536.
[27] H. De Monestrol, L. Schmirgeld-Mignot, P. Molinas-Mata, P.J.A. Molina s-Mata S. Poissonnet, G. Martin, Kinetics and mechanisms of reactive solid state deleting in the system Ag-Ni-O, Acta Mater. 49 (2001) 1655–1660.
[28] D.T. Danielson, D.K. Sparacin, J. Michel, L.C. Kimerling, Surface-energy-driven dewetting theory of silicon-on-insulator agglomeration, J. Appl. Phys. 100 (2006) 083507.